ELSEVIER

Earth and Planetary Science Letters 199 (2002) 67–79

EPSL

www.elsevier.com/locate/epsl

Lower crustal flow and the role of shear in basin subsidence: an example from the Dead Sea basin

Abdallah Al-Zoubi [a,1], Uri ten Brink [b,*]

[a] *Woods Hole Oceanographic Institution, US Geological Survey, 384 Woods Hole Road, Woods Hole, MA 02543, USA*
[b] *US Geological Survey, Woods Hole Field Center, Woods Hole, MA 02543, USA*

Abstract

We interpret large-scale subsidence (5–6 km depth) with little attendant brittle deformation in the southern Dead Sea basin, a large pull-apart basin along the Dead Sea transform plate boundary, to indicate lower crustal thinning due to lower crustal flow. Along-axis flow within the lower crust could be induced by the reduction of overburden pressure in the central Dead Sea basin, where brittle extensional deformation is observed. Using a channel flow approximation, we estimate that lower crustal flow would occur within the time frame of basin subsidence if the viscosity is $\leq 7\times10^{19}$–1×10^{21} Pa s, a value compatible with the normal heat flow in the region. Lower crustal viscosity due to the strain rate associated with basin extension is estimated to be similar to or smaller than the viscosity required for a channel flow. However, the viscosity under the basin may be reduced to 5×10^{17}–5×10^{19} Pa s by the enhanced strain rate due to lateral shear along the transform plate boundary. Thus, lower crustal flow facilitated by shear may be a viable mechanism to enlarge basins and modify other topographic features even in the absence of underlying thermal anomalies.

Keywords: lower crust; crustal thinning viscosity; subsidence; Dead Sea Rift; pull-apart basins

1. Introduction

Large subsidence with little attendant brittle deformation of the sedimentary section, deposited shortly before sea floor spreading commenced, is observed in the Iberian, Newfoundland, and NW Australian continental margins [1–3]. Lower crustal thinning by ductile deformation provides a viable mechanism for the observed regional subsidence [3]. In this model, distributed lower crust thinning across the entire width of the continental margin takes up the extension in the lower crust, whereas the upper crust is extending in a narrow region close to the future location of sea floor spreading. For this lower crustal thinning to occur over a wide area, the viscosity should be low, prompting Driscoll and Karner [3] to appeal to lower crustal heating by asthenospheric upwelling during the late stage of rifting.

Lower crustal flow has also been invoked to explain other phenomena in other tectonics settings. Deng et al. [4] and Freed and Lin [5] interpreted post-seismic relaxation of the Landers earthquake in California to indicate the presence

* Corresponding author. Tel.: +1-508-457-2396; Fax: +1-508-457-2310.
E-mail address: utenbrink@usgs.gov (U. ten Brink).

[1] On leave from the Natural Resources Authority, P.O. Box 7, Amman, Jordan.

0012-821X/02/$ – see front matter
PII: S0012-821X(02)00540-X

of lower crustal viscoelastic flow. Kruse et al. [6] explained the absence of large differences in the Bouguer gravity anomaly and the topography between the extended Basin and Range Province near Lake Mead, NV, USA, and the unextended Colorado Plateau by ductile flow in the lower crust. Kusznir and Matthews [7] explained the absence of crustal roots under old Variscan and Caledonian mountain belts by outward flow in a low viscosity channel in the lower crust in combination with other factors. Clark and Royden [8] proposed that variations in topographic gradients surrounding the Tibetan Plateau are due to variations in viscosity among the various provinces surrounding the plateau. In this paper, we use basin stratigraphy to propose that strain partitioning with depth between the upper and lower crust occurs also in small intracontinental basins under normal thermal conditions. Specifically, we examine the style of deformation due to north–south extension along the axis of the Dead Sea basin, a large pull-apart basin along the Dead Sea transform plate boundary (Fig. 1).

Left-lateral motion of $\sim$105 km took place along the Dead Sea plate boundary since the middle Miocene [9,10]. The Dead Sea basin is 135 km long, 10–20 km wide [11], and at least 8.5 km deep [12]. The basin is surrounded and underlain by several km of early Cenozoic, Mesozoic and Paleozoic sedimentary rocks, which are in turn underlain by Precambrian crystalline crust. The Mesozoic and early Cenozoic rocks were deposited at a passive continental margin setting and were gently folded by a compressional event during the latest part of the Mesozoic and the early Cenozoic. The thermal structure of the underlying crust is probably quite normal. Heat flow in the surrounding areas is 45–53 mW/m^2 [13,14], and the hot springs and locally elevated heat flow in the northern part of the basin are likely the result of meteoric water circulation along the border faults [15]. An average long-term strain rate of 2.1×10^{-15}–7.2×10^{-16} s^{-1} can be estimated from the stretching factor for the basin ($\beta=1.19$–1.34; [11]), assuming that the basin started forming 5–15 Ma. Gravity data indicate that basin extension is confined to the crust [11]. Recent seismic evidence supports the gravity interpretation and indicates that the Moho is not elevated under the basin by more than 2 km [16]. Thus, the crust of the Dead Sea basin represents an example of a deformed continental crust under extension.

This study concentrates on the southern part of the basin (Fig. 1), where the basin fill is generally free of evaporites, and the basement is clearly imaged. Seismic data from the central part of the Dead Sea were previously analyzed to determine the structure of the basin [12,17–21]. The central part of the Dead Sea is deeper than 6 km and the seismic data seldom provide clear images of the basement (basement is used to describe all the strata underlying the middle Miocene to Holocene basin fill). In addition, this part is underlain by a salt layer, which may decouple the overburden deformation from the deformation of the basement [18]. The northern Dead Sea, which is occupied by a saline lake, is probably less deep, but was only imaged with a shallow penetrating single-channel seismic system [22].

2. Interpretation of seismic data

The geophysical data sets used in the study consist of seismic reflection lines, gravity data, and data from several boreholes (Fig. 1). Previous interpretations of the subsurface geology had to rely on cross-lines across only one half of the basin and on lines oriented obliquely to the axis of the basin, because of the location of the international border between Jordan and Israel. Here we present a 32-km-long line along the axis of the basin, Line VWJ-8 (Fig. 2), and a composite

→

Fig. 1. (A) Outline of the Dead Sea transform plate boundary and the main strike–slip faults (modified from [19]). (B) Location map of the seismic lines (red lines) and boreholes used for interpretation, superimposed on shaded-relief image of the Dead Sea basin [42]. Heavy red lines – locations of Figs. 2 and 3. Blue dashed dotted line – 1967 coastline of the Dead Sea (after [22]). Location of Miocene outcrops is from [26].

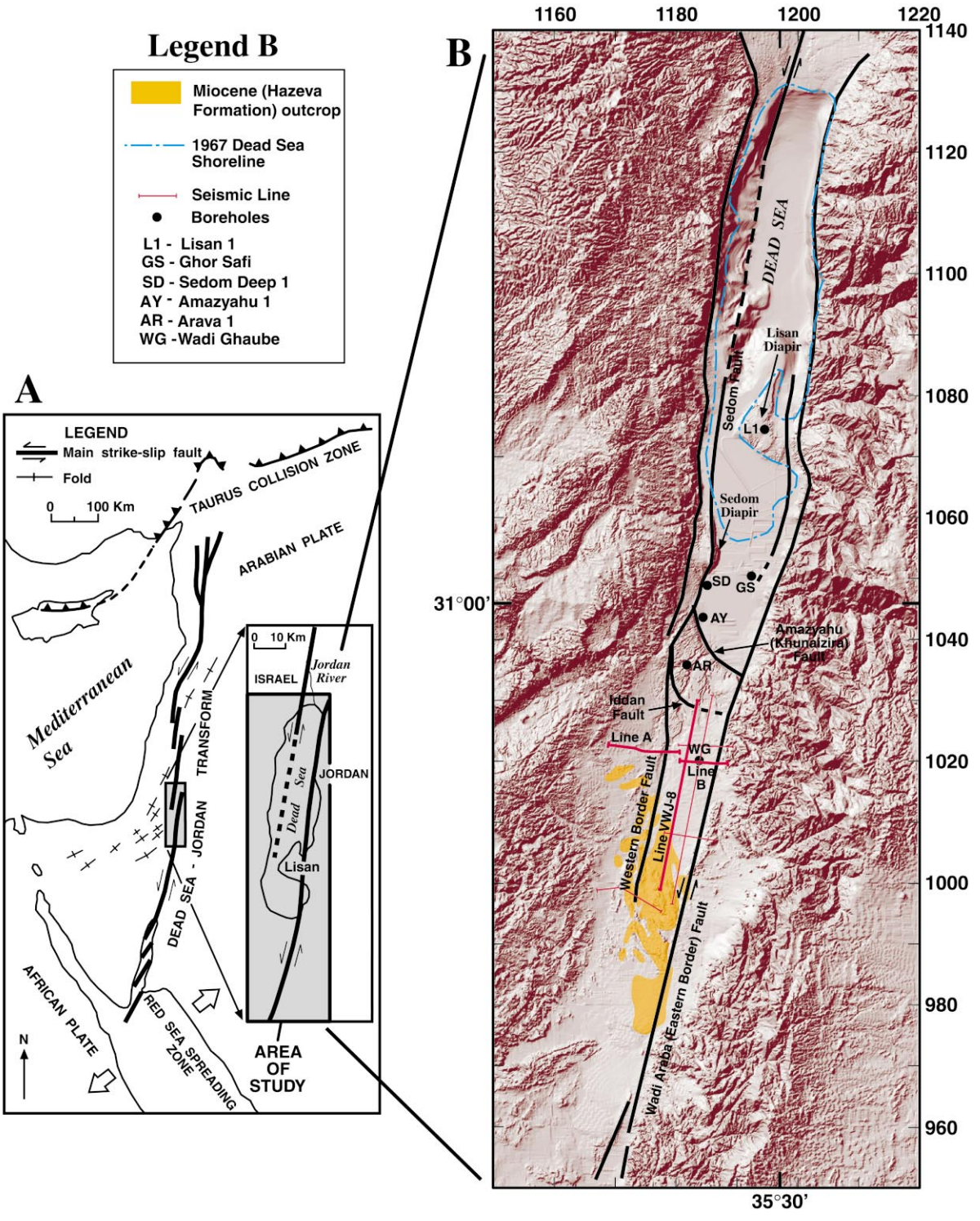
Legend B
Miocene (Hazeva Formation) outcrop
1967 Dead Sea Shoreline
Seismic Line
Boreholes
L1 - Lisan 1
GS - Ghor Safi
SD - Sedom Deep 1
AY - Amazyahu 1
AR - Arava 1
WG - Wadi Ghaube
A
LEGEND
Main strike-slip fault
Fold
0 100 Km
TAURUS COLLISION ZONE
ARABIAN PLATE
Mediterranean Sea
DEAD SEA - JORDAN TRANSFORM
AFRICAN PLATE
RED SEA SPREADING ZONE
N
0 10 Km
ISRAEL
Jordan River
JORDAN
Dead Sea
Lisan
AREA OF STUDY
B
1160
1180
1200
1220
1140
1120
1100
1080
1060
1040
1020
1000
980
960
31°00'
35°30'
DEAD SEA
Lisan Diapir
Sedom Fault
L1
Sedom Diapir
SD
GS
AY
AR
Amazyahu (Khunaizira) Fault
Iddan Fault
Line A
WG
Line B
Western Border Fault
Line WWJ-8
Wadi Araba (Eastern Border) Fault

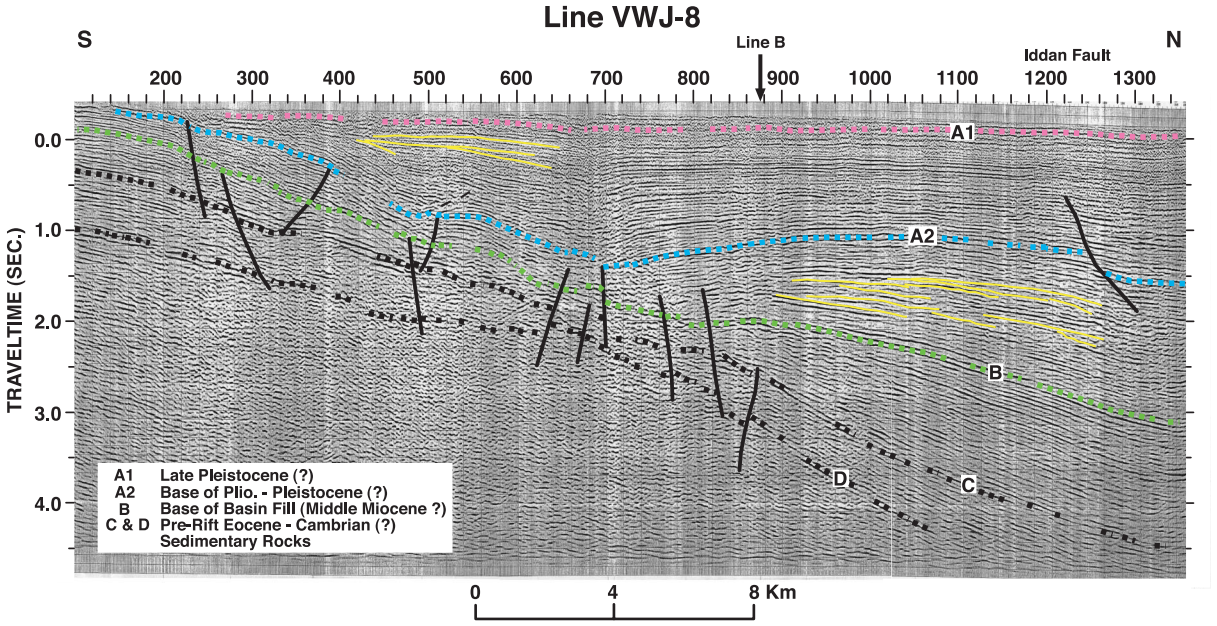

Fig. 2. Seismic Line VWJ-8. The dotted lines show interpreted stratigraphic unit boundaries. Horizon B is interpreted as the base of Miocene to recent sediments that fill the Dead Sea basin. Horizon D is tentatively interpreted as the top of crystalline basement. Yellow lines – interpreted prograding sequences of lacustrine deposits. Heavy lines – faults. Heavy dashed line – possible landslide.

cross-section across the entire basin (Fig. 3). These lines are part of a larger data set collected during the past 15 yr for oil and water exploration.

Interpretation of the seismic data was based on the lithostratigraphic data obtained from commercial boreholes in the area, Amazyahu 1, Arava 1 (e.g. [20]) and Wadi Ghuabe (I. Qabbani, personal communication, 2000). Dating of the sedimentary fill in the southern Dead Sea basin is inherently ambiguous because the sediments are largely terrestrial and lack diagnostic fauna. Arava 1 borehole, located 7 km northwest of the northern end of Line VWJ-8, was drilled in 1959. It penetrated 2650 m of basin fill, consisting of fluvial and lacustrine deposits, and did not reach the basement. Palynological data [23] indicate that the bottom 2450 m of the hole is of Miocene age (Hazeva Formation). Lithological comparison with units exposed outside the basin indicates, however, that only the bottom 2250 m of the basin is of Miocene age [24], and seismic stratigraphic correlation with seismic lines and boreholes farther north within the Dead Sea suggests that only the bottom 2000 m of the basin is comprised of undifferentiated Miocene and Pliocene sediments [20]. The Wadi Ghuabe borehole, located on Line B 2.3 km east of Line 8, was drilled in 1989. It penetrated 3200 m of basin fill sediments and did not reach basement. Interpretation indicates that the borehole consists of more than 680 m of Miocene sediments, 850 m of possibly Pliocene sediments, and about 1700 m of Quaternary sediments. We interpret the seismic data using the Wadi Ghuabe borehole, but the interpretation of the two boreholes is in fact not contradictory. The sequence bounded by horizons A2 and B (Fig. 2) which corresponds to Miocene sedimentary rocks according to Wadi Ghuabe borehole, thickens northward, and is about 2.2 km thick at the north end of Line VWJ-8 and others parallel lines in the vicinity of Arava 1 borehole. Interpretation of pre-rift (pre-Miocene) sediments is based solely on outcropping rock units in the vicinity of the rift (e.g. [25]).

The most striking feature on the seismic lines,

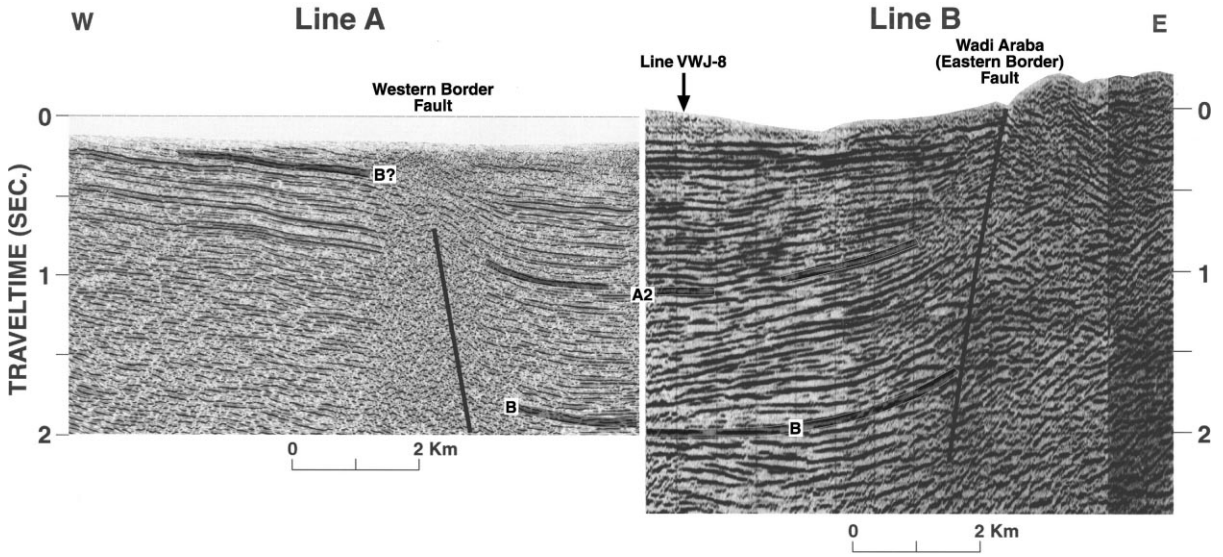

Fig. 3. Seismic lines A and B showing a cross-section of the southern part of the Dead Sea basin. Gray lines – interpreted stratigraphic unit boundaries. See Fig. 2 for further details.

which run parallel to the basin's axis, is the gradual thickening of the sedimentary section from south to north. For example, the syn-rift sedimentary section in Line VWJ-8 (above horizon B) thickens from 0.3 to 3.1 s two-way travel time (TWT) (>5 km) at the northern end of this line some 32–35 km away without major fault offsets (Fig. 2). In addition, the region of subsidence appears to have expanded southward with time.

The stratigraphic unit enclosed by Horizons A1 and A2 thickens northward toward SP 710 and is characterized by prograding sequences in the upper part of the unit and a possible landslide in the lower part of the unit. These suggest a relatively steep north-facing slope toward a depocenter at SP 710. A cross-line at SP 490 on Line VWJ-8 (Fig. 1) shows several construction mounds, which probably resulted from the stacking of valley floor sands at a hydraulic gradient change or knick point in the basin profile.

The unit bounded by horizons B and A2 thickens uniformly and gradually northward from SP 710 on Line VWJ-8 (Fig. 2). Prograding sequences within this unit at SP 900–1300 attest to increasing subsidence toward the north. Reflector A2, the unit's upper boundary, reaches the surface south of SP 160 on Line VWJ-8. The surface rocks in this area are part of the Miocene Hazeva Formation (Fig. 1; [26]), suggesting that the unit, bounded by reflectors B and A2, is part of the Miocene basin fill. The projected synthetic seismogram of Wadi Ghuabe borehole onto Line VWJ-8 confirms the identification of this unit as being of Miocene age. The Miocene sequence maintains a relatively constant thickness south of SP 710. This part was probably part of Miocene Hazeva Formation outcrops encountered outside the basin and even outside the topographic depression of the Dead Sea transform.

Horizon B is probably the basement, i.e. the base of the sedimentary fill during the development of the Dead Sea basin. It is an erosional unconformity, as indicated by the truncation of underlying strata at SP 340–400 and at SP 800–920 on Line VWJ-8. Based on the geology in the areas surrounding the central and southern Dead Sea basin, the reflections underlying Horizon B represent Eocene to Cambrian age sediments with a total thickness of 2–3 km [25–27]. The seismic sections show that the pre-rift sedimentary section in the vicinity of SP 710 was locally deeply eroded prior to or during the initial stages of basin development. The location of eroded sediments is coincident with the area of local depo-

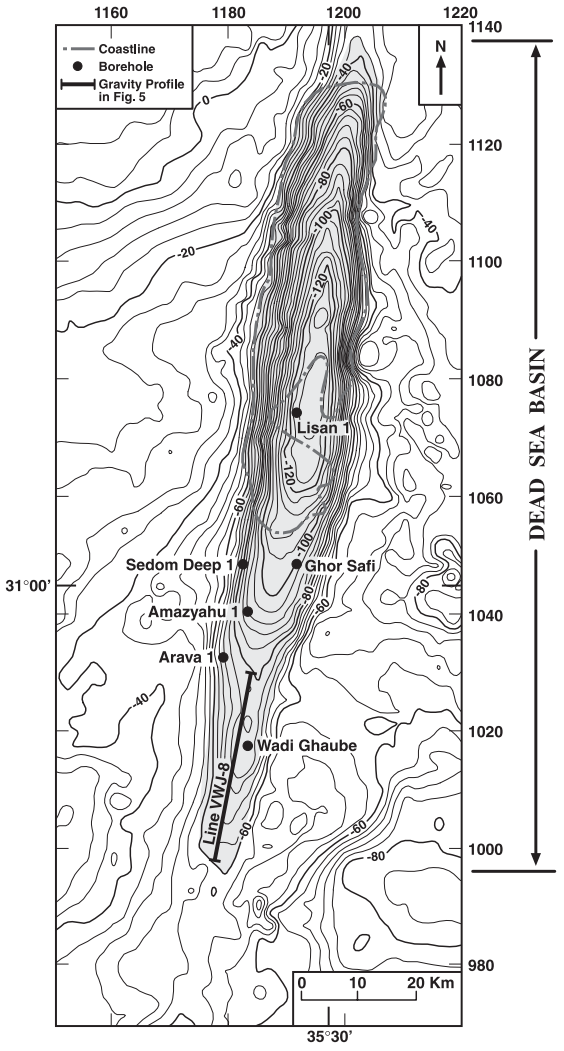

Fig. 4. Bouguer gravity anomaly map of the Dead Sea basin. Contour interval is 4 mGal. Location of the gravity profile in Fig. 5. Dashed–dotted line – 1967 coastline of the Dead Sea (after [22]). Black dots – location of wells.

center higher up in the basin fill. It thus appears that the area was first activated in compression and later reactivated in extension.

East–west oriented seismic lines A and B across this part of the Dead Sea basin show a full graben structure bounded on the east and the west by steeply dipping faults (Fig. 3). The basin is narrow – 7 km near the surface. Reflectors are slightly tilted toward the center of the basin from both the east and the west, probably as a result of alluvial fan deposition within a subsiding full graben. The eastern border of the basin, known as the Arava Fault, reaches the surface, and separates coherent basin fill reflections from chaotic bedrock to the east. This fault trace appears to be active as it offsets young alluvial fans and archeological sites (e.g. [28]). The western border fault appears on seismic Line A as a 750-m-wide zone of chaotic reflections. Reflections are pulled up along the fault trace below 0.4 s TWT, indicating that the fault was active throughout much of the basin history. However, at present the western boundary fault is buried. Coherent reflections outside the basin (west of the fault) tilt gently toward the basin. The uppermost part of this coherent reflection sequence is probably the Miocene Hazeva Formation, which is exposed at the surface. The band of strong reflectivity extending to a depth of 0.6 s TWT was interpreted farther south to represent Eocene to Cretaceous carbonate rocks [24].

3. Interpretation and modeling the gravity data

The gravity map of the area (Fig. 4), which was derived from a joint Jordanian–Israeli gravity data base [29], shows a narrow (<10 km) anomaly starting close to the southern end of the seismic profiles, and becoming more negative to the north. However, halfway north along Line VWJ-8, the anomaly flattens. We modeled the gravity anomaly along Line VWJ-8 by converting the seismic profile to depth (Fig. 5) using the sonic log of Wadi Ghuabe borehole (I. Qabbani, personal communication, 2000). Specifically, we used an average of 2.5–3 km/s for the first 1 s TWT (upper part of Pleistocene), 3.6 km/s for the lower part of Pleistocene sediments, 4 km/s for Pliocene and 4.6 km/s for the Miocene sequence. The southern half of the profile can be fit well with a two-dimensional model, but the northern half cannot. We interpret this misfit to be caused by the effect of high-density pre-rift rocks along the eastern and western boundaries. This effect becomes more significant as the basin deepens and the basin width (7 km) becomes comparable to its depth (>5 km). To take this effect into account,

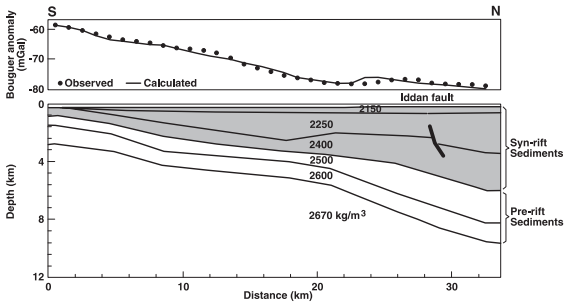

Fig. 5. Observed and calculated gravity profile over seismic Line VWJ-8. The shaded layers represent syn-rift sediments. The RMS difference between the observed and calculated gravity values is less than 2 mGal.

we modeled the gravity profile using a 'two and a half'-dimensional model that allows for a density change at a specified distance perpendicular to the profile. We assumed a 2.5-km-thick, pre-rift sedimentary section with a density of 2550 kg/m^3 overlying crystalline basement starting 3 km west of the profile and a crystalline basement with a density of 2670 kg/m^3 starting 4 km east of the profile. Densities for the basin fill were derived from well logging carried out in Sedom Deep 1 [30,31] and from Wadi Ghuabe well (I. Qabani, Personal communication, 2000). The density of pre-rift sediments and the crystalline basement were derived from well data in the surrounding areas of Jordan and from samples collected in the southern part of Jordan [32].

By accounting for density changes at the basin's eastern and western boundaries, we can obtain a satisfactory fit between the observed gravity profile along seismic Line VWJ-8 and the calculated anomaly from the depth-converted profile. The basin fill in the gravity model includes the layers with densities of 2400 kg/m^3 corresponding to Miocene Hazeva Formation, and 2250 and 2150 kg/m^3 corresponding to the Plio–Pleistocene section. The basin reaches a maximum thickness of 6 km at the northern edge of the profile.

4. Discussion

The major feature observed in the longitudinal seismic profiles is the sagging of the southern part of the Dead Sea basin toward the north without major offsets in the basin fill or in the underlying strata. The basin sag increases from zero to more than 5 km over the 35-km-long profile. The sag may have expanded southward with time, as indicated by the stratigraphy. In cross-section, the sag is symmetric and is confined by steeply dipping western and eastern boundary faults. This geometry is unusual for pull-apart basins (e.g. [33]) and is probably indicative of the extension process that created the Dead Sea basin.

ten Brink et al. [11] interpreted the gravity map over the entire length of the Dead Sea basin to indicate that the basin sags toward the center and is not bounded by faults at its ends. The present study verifies their interpretation of the gravity data. ten Brink et al. [11] suggested that the basin's shape is controlled by stretching of the entire (brittle and ductile) crust along its long axis. The sagging indicates that the upper crust lost its foundation over a wider area than just the deepest part of the basin, which could happen if the upper crust has a finite rigidity and the ductile lower crust also stretched and necked [11]. Katzman et al. [34] generated the sagging using a three-dimensional boundary-element numerical model of overlapping en-echelon strike–slip fault in an elastic medium. In their model, the sagging is caused by shear traction applied to the base of the brittle upper crust, which is distributed horizontally over 20–40 km across the Dead Sea transform [34]. The sagging is due to necking of the upper crust, caused by the north–south stretching, and is small in amplitude relative to the thickness of the layer. Our observations show over 5 km of sagging, which is about 1/3 of the thickness of the upper crust. It is, thus, unlikely that the sagging is entirely due to necking of the upper crust.

Gravity models across the basin [11] and across the transform outside the basin [35], as well as preliminary seismic refraction results across the southern part of the Dead Sea basin [16], show that the Moho is not elevated by more than 2 km beneath the basin. Magmatic underplating does not appear to be a viable mechanism for producing a flat Moho in this area, because of the normal heat flow (45–53 mW/m^2 [13,14]) and the paucity of volcanic outcrops (e.g. [26]). Our pre-

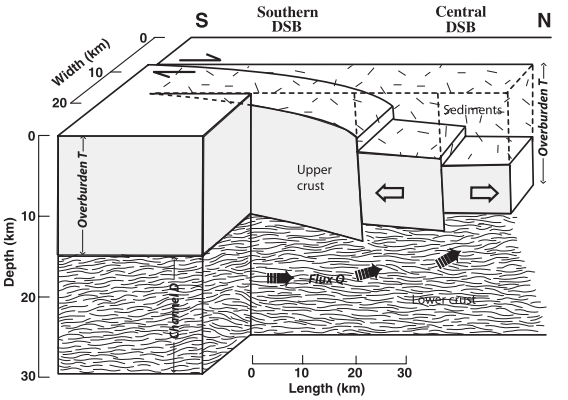

Fig. 6. Conceptual model for the development of the Dead Sea basin. Lower crustal flow toward the central Dead Sea basin (DSB) as a result of upper crustal extension and distributed lower crustal thinning causes the sagging of the southern DSB.

ferred interpretation is that lower crustal flow appears to detach upper crustal deformation from any deformation that might be occurring in the mantle lithosphere. As mentioned in Section 1, lower crustal flow may be a ubiquitous feature of late-stage rifting in continental margins. In the Basin and Range Province of the western USA, an area of high geothermal gradient, lower crustal flow was invoked to explain the relatively flat Moho beneath this highly extended terrain [36]. Here we propose that lower crustal flow can be initiated also under normal geothermal conditions as probably exist in the vicinity of the Dead Sea basin.

4.1. Channel flow

Lower crustal flow can be induced by localized stretching of the upper crust in the central Dead Sea basin (Fig. 6). Stretching of the upper crust reduces the overburden pressure of the underlying lower crust, which drives the ductile flow from the surrounding areas into the area of localized stretching. Laboratory experiments (e.g. [37]) suggest that the lower crust deforms under lower stresses than the overlying crust and the underlying mantle, because lower crustal rocks are less mafic than mantle rocks, whereas temperatures in the lower crust are higher than in the upper crust. Lower crustal flow can therefore be approximated as a flow in a low-strength channel (e.g. [6]). Channel flow occurs in response to pressure differences along the channel. Pressure difference can be induced by variations in the overburden, i.e. the thickness of the upper crust, in response to extension. The central Dead Sea exhibits brittle deformation and is filled by $\sim$9 km of syn-rift sediments and air. This extension has likely created a pressure gradient between the southern end of the Dead Sea, where the overburden is a 15-km-thick upper crust, and the central part of the basin some 80 km away, where the overburden consists of 6 km crust, $\sim$8.4 km of sediments and 0.6 km of air. The effective overburden thickness in the central part of the basin, assuming average sediment density of 2250 kg/m^3, is equivalent to a 13-km-thick upper crustal column with a density of 2670 kg/m^3. The magnitude of the pressure gradient is, however, not important in our simple analytical calculation of channel flow viscosity as will be shown below. The estimated channel flow viscosity is the viscosity required for the flow to fully respond to the pressure gradient over the time period of basin formation.

The flow velocity, u, of a Newtonian fluid with a viscosity, μ, in a channel of thickness D with a pressure gradient of $\mathrm{d}p/\mathrm{d}x$, and zero velocity at the top and bottom of the channel [8], is:

$$u = \frac{1}{2\mu}\frac{\mathrm{d}p}{\mathrm{d}x}(z^2 - hz) \tag{1}$$

The flux, Q, of material through the channel [6] is obtained by integrating the velocity over the channel thickness, D:

$$Q = \int_0^D u(z)\mathrm{d}z = \frac{D^3}{12\mu}\frac{\mathrm{d}p}{\mathrm{d}x} \tag{2}$$

The pressure gradient is the difference in the effective overburden thickness, T, between the center of the basin and its southern edge [6,8]:

$$\frac{\mathrm{d}p}{\mathrm{d}x} = \rho g\frac{\mathrm{d}T}{\mathrm{d}x} \tag{3}$$

Assuming conservation of mass, changes in the effective overburden thickness with time can be related to changes in flux by:

$$\frac{dT}{dt} = \frac{dQ}{dx} \tag{4}$$

Using Eq. 2, and assuming a constant viscosity along the channel, we can rewrite Eq. 4 as:

$$\frac{dT}{dt} = \frac{D^3}{12\mu}\rho g\frac{d^2T}{dx^2} \tag{5}$$

Re-arranging Eq. 5 we can calculate the viscosity, μ:

$$\mu = \frac{D^3}{12}\rho g\left(\frac{1}{dT/dt}\right)\frac{d^2T}{dx^2} \tag{6}$$

To get an estimate of the channel viscosity under the Dead Sea basin, we make the following simplifying substitutions: we substitute the thickness gradient with the difference in the effective overburden thickness, ΔT, between the southern and central Dead Sea. We further substitute the thickness variation with time with the difference in effective overburden thickness over the entire period of basin subsidence (Table 1). Eq. 6 is then simplified to the form:

$$\mu = \frac{D^3}{12}\rho g\left(\frac{\Delta t}{\Delta T}\right)\frac{\Delta T}{L^2} \tag{7}$$

where L is the distance between the central deepest part of the basin and its southern edge. Note that the effective thickness difference cancels out and Eq. 7 reduces to:

$$\mu = \frac{D^3}{12}\rho g\frac{\Delta t}{L^2} \tag{8}$$

Namely, the viscosity required to equilibrate lateral variations in upper crustal overburden via a channel flow in the lower crust depends on the channel thickness, D, the length scale of the flow, L, and the time. Despite the cubic dependence of the viscosity on the channel depth, D, viscosity estimates are often more sensitive to the length scale and the time span, because these parameters may vary by two orders of magnitude or more, whereas channel width usually varies by no more than 5–10 km.

Using Eq. 8 and the parameters in Table 1, we estimate that channel flow in the lower crustal can take place if the viscosity of the lower crust under the Dead Sea basin is lower or equal to 5.4×10^{20} Pa s. Using acceptable variations to these parameters (see Table 1), we estimate the upper bound viscosity for channel flow to range between 6.8×10^{19} and 1.4×10^{21} Pa s.

4.2. Estimated lower crust viscosity and the effect of shear

An estimate of lower crustal viscosity under the Dead Sea basin can be obtained if the strain rate and lower crustal temperatures are known. Laboratory experiments suggest that lower crustal rocks deform by thermally activated creep mechanisms [37]:

$$\dot{\varepsilon} = A(\sigma_1-\sigma_3)^n e^{-Q/RT} \tag{9}$$

Table 1
Values of parameters used to calculate lower crustal linear viscosity in the Dead Sea basin by the channel flow assumption, other reasonable values for these parameters and their effects on the calculated viscosity

Parameter	Preferred value	Other values	Multiply μ_0 by	Other values	Multiply μ_0 by
D	15 km	7.5 km	0.125	20 km	2.37
L	80 km	50 km	2.56		
Δt	15 Myr	5 Myr	0.333	10 Myr	0.666
ρ	2670 kg/m^3				
g	9.8 m/s^2				

μ_0 – viscosity of 5.4×10^{20} Pa s, calculated using the preferred values given in the first column.

Table 2
Experimentally determined constants for power law rheology for the lower crust

	Maryland diabase [40]	Pikwitonei granulite [41]
n	4.7	4.2
Q	4.85×10^5 J/mol	4.45×10^5 J/mol
A	8×10^6 Pa s	1.4×10^{10} Pa s

where T is the temperature in K, Q is the activation energy, R is the universal gas constant, and A and n are constants (Table 2). By substituting deviatoric stress by the product of strain rate and effective viscosity, μ_{eff}:

$$(\sigma_3-\sigma_1) = 2\mu_{\text{eff}}\dot{\varepsilon} \tag{10}$$

We can write the power law rheology in terms of the effective viscosity, as [6]:

$$\mu_{\text{eff}} = \frac{\dot{\varepsilon}^{(1/n)-1}e^{Q/nRT}}{2A^{1/n}} \tag{11}$$

To estimate crustal temperatures with depth, $T(z)$, from the observed heat flow, q, we use Lachenbruch and Sass' [38] relationship:

$$T(z) = [(q-HA_0)z + H^2A_0(1-e^{-z/H})]/k \tag{12}$$

which accommodates the exponential decrease of radiogenic heat production with depth (see Table 3). Using the values in Table 3 and the observed heat flow for the region (45–53 mW/m^3), we calculate the temperature range to be between 240 and 305°C at a depth of 20 km and between 270 and 366°C at a depth of 30 km.

The average strain rate due to the basin extension and subsidence is 2.1×10^{-15}–7.2×10^{-16} s^{-1} (see Section 1). Using the extreme bounds of the estimated temperatures (240–366°C) and strain rates, and the experimentally determined rheological constants of Maryland diabase (Table 2), we estimate the effective viscosity to be 1.7×10^{18}–6.9×10^{20} Pa s. This range of viscosities overlaps the range of viscosities required to generate channel flow due to differential overburden. Hence, channel flow may or may not occur due to north–south extension along the basin.

Lower crustal viscosity may be considerably smaller, however, if we consider shear, because shear strain rate due to the strike–slip motion is one to two orders of magnitude higher than the strain rate calculated from extension and subsidence. The rate of motion along the Dead Sea transform is $\sim$5 mm/yr, and if the lateral motion is accommodated in the lower crust in a 15-km-wide shear zone (the rate is even faster for a narrower zone), then the strain rate is 1.1×10^{-14} s^{-1}. Using the extreme bounds of the estimated temperatures and the experimentally determined rheological constants of Maryland diabase (Table 2), we estimate the effective viscosity needed to sustain the shear to be 4.6×10^{17}–5.4×10^{19} Pa s. The true rheological parameters for the lower crust are, in fact, poorly known. For example, using parameters for Pikwitonei granulite (Table 2) gives an order of magnitude lower viscosity than by using the Maryland diabase parameters. Regardless, the calculated viscosity due to lateral shear along the Dead Sea transform is considerably lower than the viscosity required for channel flow in the lower crust, and this increases the likelihood that channel flow is indeed significant under the Dead Sea basin.

The estimated viscosity due to shear is similar to the value of lower crustal viscosity in the Mojave Desert, CA, USA (10^{18}–10^{19} Pa s), required to explain post-seismic deformation of the Landers earthquake [4], uplift and tilt of Quaternary lake sediments [39], and delayed triggering of the 1999 Hector Mine earthquake [5]. The low viscosity in the Mojave Desert has been attributed to the thermal anomaly of the Basin and Range

Table 3
Parameters used to calculate crustal temperatures [38]

K	Thermal conductivity	2.5 W/m/K
A_0	Surface value of radiogenic heat production	1.5 μW/m^3
H	Logarithmic decrement of heat production	15 km
q	Heat flow	45–53 mW/m^2

Province [4]. We propose here that lower crustal shear acts to weaken the crust and promote ductile flow even in the absence of a thermal anomaly.

5. Conclusions

We present newly released seismic profiles from the southern part of the Dead Sea basin, which shed light on the extension processes involved in the formation of this large pull-apart basin. The seismic profiles show gradual thickening of the basin from south to north without major vertical offsets in either the basin fill or the underlying strata. At the southern edge of the basin, the thickness is zero, but 35 km to the north, the fill expands to more than 5 km. The stratal geometry indicates a southward expansion of the subsidence with time, which caused the basin to lengthen. In cross-section, the basin is 7 km wide, fault-bounded on both its eastern and western sides, and the internal stratigraphy indicates symmetrical subsidence. We propose that the observed subsidence is due to necking of the lower crust over a longer area than is defined by brittle deformation. Lower crustal flow may be driven by the thinning of the brittle overburden in the central part of the basin and possibly by thinning of the lower crust in response to north–south stretching. Using a channel flow assumption, lower crustal flow in response to a gradient in the overburden pressure will occur within the time frame of basin development if lower crustal viscosity is $\leq 6.8\times10^{19}$–1.4×10^{21} Pa s. Lower crustal viscosity under the Dead Sea basin can be estimated from the regional surface heat flow and from strain rate. The estimated viscosity using the strain rate calculated from basin subsidence due to north–south extension is similar or slightly smaller than the viscosity required for a channel flow. Hence, a channel flow may or may not occur even under extension-only strain rate. Strain rates due to shear motion along the Dead Sea transform plate boundary are considerably higher than those for basin extension, resulting in a reduced lower crustal viscosity under the basin, 4.6×10^{17}–5.4×10^{19} Pa s. Thus, lateral shear along the Dead Sea transform increases the likelihood that lower crustal flow is a significant factor in the subsidence of the Dead Sea basin. In contrast to the Mojave Desert, CA, USA, where a similar range of lower crustal viscosities is inferred, heat flow in the Dead Sea region is close to the continental average. We therefore propose that lateral shear and high extensional strain rates may facilitate lower crustal flow even in areas of normal thermal regime.

Acknowledgements

A.A.-Z., tenure at the Woods Hole Oceanographic Institution, was funded by the Fulbright Exchange Program of the US Government. Special thanks to the Minister of Energy and Mineral Resources and the General Director of the Natural Resources Authority (NRA), Jordan, for their permissions to carry this study outside Jordan. We thank the Earth Science Administration in the Ministry for National Infrastructure, Israel, for permission to publish Line A, and Dr. Yair Rotstein, Geophysical Institute of Israel, for providing this line. A.A.-Z. would like to thank the USGS/Woods Hole Field Center for opening their data archive for this study and for using their facilities, and the Woods Hole Oceanographic Institution/Department of Geology and Geophysics for their hospitality. The support of Mr. Alan McNamara, head of the Fulbright office in Jordan, and his staff is greatly appreciated. Reviews by Sarah Kruse, Jian Lin, Ingo Pecher, an anonymous, and the editor Scott King helped to improve the manuscript. J. Zwinakis drafted the figures. *[SK]*

References

[1] A.J. Tankard, H.J. Welsink, Extensional tectonics and stratigraphy of Hibernia oil field, Grand Banks, Newfoundland, AAPG Bull. 71 (1987) 1210–1232.

[2] G. Boillot, E.L. Winterer, A.W. Meyer, J. Applegate, M. Baltuck, J.A. Bergen, M.C. Comas, T.A. Davies, K.W. Dunham, C.A. Evans, J. Girardeau, D. Goldberg, J.A. Haggerty, L.F. Jansa, J.A. Johnson, J. Kasahara, J.-P. Loreau, E. Luna, M. Moullade, J.G. Ogg, M. Sarti, J. Thurow, M.A. Williamson, E.K.E. Mazzullo, Drilling

on the Galicia margin; retrospect and prospect, Proceedings of the Ocean Drilling Program, Scientific Results, Vol. 103, 1988, pp. 809–828.
[3] N.W. Driscoll, G.D. Karner, Lower crustal extension across the northern Carnarvon Basin, Australia; evidence for an eastward dipping detachment, J. Geophys. Res. 103 (1998) 4975–4991.
[4] J. Deng, M. Gurnis, H. Kanamori, E. Hauksson, Viscoelastic flow in the lower crust after the 1992 Landers, California, earthquake, Science 282 (1998) 1689–1692.
[5] A.M. Freed, J. Lin, Delayed triggering of the 1999 Hector Mine earthquake by viscoelastic stress transfer, Nature 411 (2001) 180–183.
[6] S. Kruse, M.K. McNutt, J. Phipps-Morgan, L. Royden, B.P. Wernicke, Lithospheric extension near Lake Mead, Nevada; a model for ductile flow in the lower crust, J. Geophys. Res. 96 (1991) 4435–4456.
[7] N.J. Kusznir, D.H. Matthews, Deep seismic reflections and the deformational mechanics of the continental lithosphere, in: M.A. Menzies, K.G. Cox (Eds.), International Conference on Oceanic and Continental Lithosphere; Similarities and Differences, J. Petrol., Egham, 1988, pp. 63–87.
[8] M.K. Clark, L.H. Royden, Topographic ooze; building the eastern margin of Tibet by lower crustal flow, Geology 28 (2000) 703–706.
[9] A.M. Quennell, The structural and geomorphic evolution of the Dead Sea rift, Q. J. Geol. Soc. Lond. 114 (Part 1) (1958) 1–24.
[10] R. Freund, Z. Garfunkel, I. Zak, M. Goldberg, T. Weissbrod, B. Derin, The shear along the Dead Sea rift, Philos. Trans. R. Soc. Lond. Ser. A 267 (1970) 107–130.
[11] U.S. ten Brink, Z. Ben-Avraham, R.E. Bell, M. Hassouneh, D.F. Coleman, G. Andeasen, G. Tibor, B. Coakley, Structure of the Dead Sea pull-apart basin from gravity analysis, J. Geophys. Res. 98 (1993) 21887–21894.
[12] A. Al-Zoubi, U.S. tenBrink, Salt diapirs in the Dead Sea basin and their relationship to Quaternary extensional tectonics, Mar. Petrol. Geol. 18 (2001) 779–797.
[13] S.P. Galanis Jr., J.H. Sass, R.J. Munroe, M. Abu-Ajamieh, Heat flow at Zerqa Ma'in and Zara and a geothermal reconnaissance of Jordan, USGS Open-File Report 86-631, 1–110, 1986.
[14] Y. Eckstein, G. Simmons, Measurements and interpretation of terrestrial heat flow in Israel, Geothermics 6 (1978) 117–142.
[15] H. Gvirtzman, G. Garven, G. Gvirtzman, Thermal anomalies associated with forced and free ground-water convection in the Dead Sea Rift valley, Geol. Soc. Am. Bull. 109 (1997) 1167–1176.
[16] M. Weber, Z. Ben-Avraham, K. Abu-Ayyash, R. El-Kelani, Desert 2000 – Multinational and interdisciplinary project to study the Dead Sea rift/Dead Sea transform, EOS Trans. Am. Geophys. Union 81 (2000) F1223.
[17] E.L. Kashai, P.F. Croker, Structural geometry and evolution of the Dead Sea–Jordan rift system as deduced from new subsurface data, Tectonophysics 141 (1987) 33–60.
[18] U.S. ten Brink, Z. Ben-Avraham, The anatomy of a pull-apart basin: Seismic reflection observations of the Dead Sea basin, Tectonics 8 (1989) 333–350.
[19] M. Gardosh, E. Kashai, S. Salhov, H. Shulman, E. Tannenbaum, Hydrocarbon exploration in the southern Dead Sea basin, in: T.M. Niemi, Z. Ben-Avraham, J.R. Gat (Eds.), The Dead Sea: The Lake and its Setting, Oxford University Press, Oxford, 1997, pp. 57–72.
[20] I. Csato, C.G.S.C. Kendall, A.E.M. Nairn, G.R. Baum, Sequence stratigraphic interpretations in the southern Dead Sea basin, Israel, Geol. Soc. Am. Bull. 109 (1997) 1485–1501.
[21] A. Al-Zoubi, H. Shulman, Z. Ben-Avraham, Seismic reflection profiles across the southern Dead Sea basin, Tectonophysics, in press.
[22] D. Neev, J.K. Hall, Geophysical investigations in the Dead Sea, Sedim. Geol. 23 (1979) 209–238.
[23] A. Horowitz, Palynological evidence for the age and rate of sedimentation along the Dead Sea Rift and structural implications, Tectonophysics 141 (1987) 107–115.
[24] Y. Bartov, Y. Avni, R. Calvo, U. Frieslander, The Zofar fault – A major intra-rift feature in the Arava rift valley, GSI Curr. Res. 11 (1998) 27–32.
[25] F. Bender, Geology of Jordan, Gebrueder Borntraeger, Berlin, 1974, 196 pp.
[26] A. Sneh, K. Ibrahim, Y. Bartov, I. Rabba, T. Weissbrod, K. Tarawneh, M. Rosensaft, Geological map of the Dead Sea rift along Wadi Araba, Joint work between Israel Geological Survey and Natural Resources Authority of Jordan, 1998.
[27] S. Wdowinski, E. Zilberman, Kinematic modelling of large-scale structural asymmetry across the Dead Sea Rift, Tectonophysics 266 (1996) 187–201.
[28] Y. Klinger, J.P. Avouac, L. Dorbath, N. Abou Karaki, N. Tisnerat, Seismic behaviour of the Dead Sea Fault along Araba Valley, Jordan, Geophys. J. Int. 142 (2000) 769–782.
[29] U.S. ten Brink, M. Rybakov, A.S. Al-Zoubi, M. Hassouneh, U. Frieslander, A.T. Batayneh, V. Goldschmidt, M.N. Daoud, Y. Rotstein, J.K. Hall, Anatomy of the Dead Sea Transform; does it reflect continuous changes in plate motion?, Geology 27 (1999) 887–890.
[30] M. Rybakov, V. Goldshmidt, L. Fleischer, Y. Rotstein, I. Goldberg, Interpretation of gravity and magnetic data from Israel and adjacent areas, Report R04/486/94, The Institute of Petroleum Research and Geophysics, Tel Aviv, 1995.
[31] M. Rybakov, V. Goldshmidt, Y. Rotstein, L. Fleischer, I. Goldberg, C. Campbell, P. Millegan, Petrophysical constraints on gravity/magnetic interpretation in Israel, Leading Edge 18 (1999) 269–272.
[32] M. Abu-Ajamieh, Geophysical survey in the southern Jordan, Natural Resources Authority, Amman, 1967, 41 pp.

[33] K. McClay, T. Dooley, Analogue models of pull-apart basins, Geology 23 (1995) 711–714.
[34] R. Katzman, U.S. ten Brink, J. Lin, Three-dimensional modeling of pull-apart basins; implications for the tectonics of the Dead Sea basin, J. Geophys. Res. 100 (1995) 6295–6312.
[35] U.S. ten Brink, N. Schoenberg, R.L. Kovach, Z. Ben-Avraham, Uplift and a possible Moho offset across the Dead Sea transform, Tectonophysics 180 (1990) 71–85.
[36] P.B. Gans, An open-system, two-layer crustal stretching model for the eastern Great Basin, Tectonics 6 (1987) 1–12.
[37] C. Goetze, B. Evans, Stress and temperature in the bending lithosphere as constrained by experimental rock mechanics, Geophys. J. R. Astron. Soc. 59 (1979) 463–478.
[38] A.H. Lachenbruch, J.H. Sass, Heat flow in the United States and the thermal regime of the crust, in: J.G. Heacock, G.V. Keller, J.E. Oliver, G. Simmons (Eds.), The Earth's Crust; its Nature and Physical Properties, Geophysical Monograph, Vail, CO, 1977, pp. 626–675.
[39] P.S. Kaufman, L.H. Royden, Lower crustal flow in an extensional setting; constraints from the Halloran Hills region, eastern Mojave Desert, California, J. Geophys. Res. 99 (1994) 15723–15739.
[40] S.J. Mackwell, M.E. Zimmerman, D.L. Kohlstedt, High-temperature deformation of dry diabase with application to tectonics on Venus, J. Geophys. Res. 103 (1998) 975–984.
[41] K.R. Wilks, N.L. Carter, D.M. Fountain, A. Boriani, Rheology of some continental lower crustal rocks, Tectonophysics 182 (1990) 57–77.
[42] J.K. Hall, The GSI digital terrain model (DTM) project completed, Curr. Res. Geol. Surv. Isr. 8 (1993) 47–50.